International Journal of Fluid Machinery and Systems
Vol. 2, No. 3, July-September 2009

Original Paper

Fluid-Oscillation Coupled Analysis for HAWT Rotor Blade (One Degree of Freedom Weak Coupling Analysis with Hinge-Spring Model)

Hiroshi Imamura[1], Yutaka Hasegawa[2], Junsuke Murata[3], Sho Chihara[4], Daisuke Takezaki[4] and Naotsugu Kamiya[3]

[1] Wind Energy Institute Co., Ltd,
Terada Building, 4-29-6 Shinbashi, Minato-ku, Tokyo, 105-0004, Japan
[2] EcoTopia Science Institute, Nagoya University
Furo-cho, Chikusa-ku, Nagoya, 464-8603, Japan
[3] Department of Mechanical Science and Engineering, Nagoya University
Furo-cho, Chikusa-ku, Nagoya, 464-8603, Japan
[4]Nissan Motor Co., Ltd.,
17-1, Ginza 6-chome, Chuo-ku, Tokyo, 104-8023, Japan

Abstract

Since large-scale commercial wind turbine generator systems such as MW-class wind turbines are becoming widely operated, the vibration and distortion of the blade are becoming larger and larger. Therefore the soft structure design instead of the solid-design is one of the important concepts to reduce the structural load and the cost of the wind turbine rotors. The objectives of the study are development of the fluid-structure coupled analysis code and evaluation of soft rotor-blade design to reduce the unsteady structural blade load. In this paper, fluid-structure coupled analysis for the HAWT rotor blade is performed by free wake panel method coupled with hinge-spring blade model for the flapwise blade motion. In the model, the continuous deflection of the rotor blade is represented by flapping angle of the hinge with one degree of freedom. The calculation results are evaluated by comparison with the database of the NREL unsteady aerodynamic experiment. In the analysis the unsteady flapwise moments in yawed inflow conditions are compared for the blades with different flapwise eigen frequencies.

Keywords: Wind Turbine, Free Wake Panel Method, Weak Coupling Analysis, Hinge-Spring Model, Yawed Inflow

1. Introduction

The manufacturing technology of the wind turbine generator systems (WTGS) has been developed rapidly, and it has made possible to produce MW-class commercial WTGS, whose rotor diameter is larger than 60m[1]. The increase of the rotor diameter brings about increased effects from the vibration and distortion of the rotor blade on its fatigue life. The WTGS installed over the complex terrain, such as in Japan, often encounters the wind environment with high turbulent intensity, which might cause serious problems such as the shortening of the blades' lifetime and failures of the drive trains due to the vibration and the distortion of the blades.

Recently a concept of soft structure design for the rotor blade and tower is attracting attentions in the wind engineering field as an alternative to the rigid structure design, since the former has possibility to reduce the unsteady structural blade load. Thus it has become important to figure out the effects of the structural oscillation on the performance of the soft-designed wind turbine.

The calculation tools used for the aerodynamic load in the design process of the wind turbine rotors are mostly based on the blade element momentum (BEM) theory. Their representatives are the calculation codes such as FAST[2] developed by the National Renewable Energy Laboratory (NREL), and Bladed[3] by Garrad Hassan & Partners. Since the BEM theory originally assumes axisymmetric flow field around the turbine rotor, the calculation models based on the BEM involves intrinsic inconsistency with the asymmetric inflow condition about the rotor axis[4]. Therefore the tools based on the BEM can't cope with the yawed inflow phenomena, although it can predict the aerodynamic load with satisfactory level of accuracy by adopting various corrections for the practical application.

Received October 10 2008; accepted for publication July 16 2009: Review conducted by Prof. Yutaka Ota. (Paper number O08031)
Corresponding author: Yutaka Hasegawa, Professor, y-hasegawa@esi.nagoya-u.ac

In order to predict the wind turbine performance precisely under yawed inflow condition[5], the calculation model should base on a physical model which can represent the unsteady effects from the inclined configuration of the wake vortices emitted from the rotor blades without using empirical constants. From this point of view, CFD[6] can be a good candidate for the matter since it can serve us precise information of the flow field around rotor blade, although its consuming time and cost prevent us from using CFD as the design tool for the wind turbine rotor.

The present study aims at developing a reliable and fast-running tool for the load estimation in the design process of the HAWT (Horizontal Axial Wind Turbine) by adopting the panel method with a free wake model, which can take the effects from the wake geometry into consideration, and viscous correction model for the aerodynamic force coefficients. For the establishment of the calculation tool with increased accuracy of the aerodynamic load prediction, the proposed calculation model would be applied to various operating conditions which involve unsteady flow phenomena around the rotor blades, and evaluate the validity of the simulated results. The computation time is about 8 hours to obtain a result of the coupled analysis by using WS (AMD Opteron 246 2.0GHz).

In this paper the flow around a horizontal axis wind turbine rotor in a yawed flow condition is analyzed by the proposed calculation model. The model includes a semi-empirical dynamic stall model developed by ONERA[8] to estimate unsteady lift force on the blade section when the angle of attack to the section fluctuates with large amplitude in high frequency.

In order to develop a tool for the soft structural design of large wind turbines, a fluid-oscillation coupled analysis model has been constructed, which can analyze the flow field around the rotor blades oscillating in the flapwise direction due to unsteady aerodynamic force on the blade. A simplified structural model with one degree of freedom is adopted in the present analysis, since the first mode oscillation is thought to be dominant in the flapwise oscillation. The analysis model and calculated results are presented, and the effects of the blade oscillation on the aerodynamic load and the rotor performance are examined in this paper.

2. Analysis Model and Calculation Method

2.1 Vortex Lattice Method with Free Wake Model

The aerodynamic load on the wind turbine rotor is calculated by using the vortex lattice method[9] based on the panel method, where the rotor blade surface is divided into quadrilateral panel elements as shown in Fig. 1. The lattice panels, which have four vortex filaments with circulation γ, represent the aerodynamic effects of the blade. The unknown quantity γ for each panel is derived by applying Neumann type boundary condition at a collocation point of each panel.

The circulation Γ around the blade surface is conserved in accordance with Kelvin's circulation theorem and the vortex panels are released from the trailing edge of the blade and shed into the wind turbine wake with the advance of time. The free wake model is applied to the advection of the vortex panels by using Euler method[9], which transfers and deform the wake vortex panel with the local velocity at respective nodal points of each panel. The wake emitted from each rotor blade of the wind turbine forms helical geometry with some roll-up near the tips for the normal operating condition.

Since the vortex lattice method assumes inviscid flow around the turbine rotor, viscous effects on the aerodynamic load on the blades are considered by using 2-D steady airfoil characteristics[9], which are usually obtained from the wind tunnel experiments. The viscous correction model can be summarized as follows.

Using the local circulation Γ obtained from the inviscid flow calculation, the inviscid local lift coefficient c_{linv} can be deduced by Kutta-Joukowski theorem as $c_{linv}=2\Gamma/U_R c$, where U_R is relative speed to the blade section, and c is the local chord length. The angle of attack α is, then, derived by using the lift slope of the linear part in the 2-D airfoil characteristics. From the angle of attack at the local section and the corresponding 2-D airfoil characteristics, we finally obtain the corrected lift coefficient c_{lvis} and the corrected drag coefficient c_{dvis}.

2.2 Dynamic Stall Model

The wind turbine operating in the open-air suffers from continuous changes in the wind speed and wind direction. Therefore, the wind turbine often encounters the yawed inflow condition[5], where the relative velocity and the angle of attack to the rotor blade change with the azimuth angle of the blade ψ defined in Fig. 1.

In the yawed inflow condition dynamic stall phenomena[6] frequently occur on the blade surface especially near the blade root. Of the many models for considering the dynamic stall, the present study adopts ONERA method[8], which is widely used for the unsteady load calculation of the wind turbine rotor. Please refer to the review article by Leishman[10], which covers the most of the dynamic stall models used for wind turbine aerodynamics.

2.3 Fluid-Oscillation Coupled Model

The blade of the HAWT rotor oscillates in the various ways, such as the torsional oscillation around the elastic axis (pitching oscillation) and the bending oscillation normal to the rotating plane (flapwise oscillation). In the present paper, the flapwise oscillation due to the aerodynamic load fluctuation was intended as the subject, and was

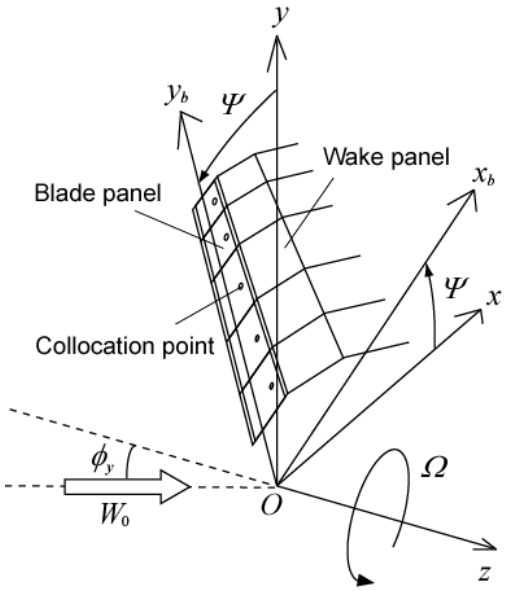

Fig. 1 Coordinate systems and vortex panels

physically and numerically modeled as follows. It can be said that the constructed model is able to analyze also the teetered wind turbine rotor[11], [12].

As shown in Fig. 2, the flapwise oscillation is represented by a simple elastic model whose center of the blade's rotational movement locates at the blade root of the rotor. It is supposed that there is the elastic hinge spring at the blade root and the other blade part is the rigid body which has the mass (inertia moment). The blade model has one degree of freedom denoted by the instantaneous flapping angle β_f, and is composed of the moment of inertia of the blade I and the spring constant of the hinge spring k, along with the structural damping coefficient c_{ab}. The driving force moment comes from the flapwise fluid moment M_f due to the aerodynamic load and the effects due to the gravity force and the centrifugal force on the blade. The equation of motion for the model is written as below,

$$I\ddot{\beta}_f + c_{ab}\dot{\beta}_f + k\beta_f - \frac{3Ig}{2R}\beta_f \cos\Omega t + \beta_f I\Omega^2 = M_f \qquad (1)$$

where the symbol '$\cdot$' represents the temporal differentiation, R is the rotor radius and g is the acceleration of gravity.

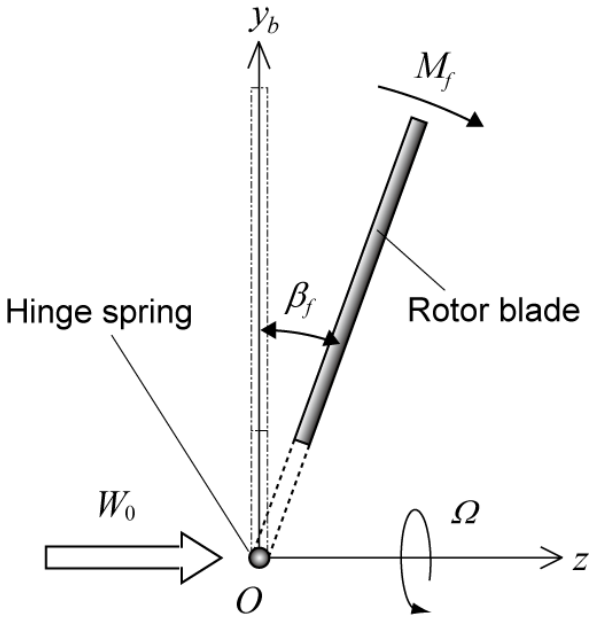

Fig. 2 Blade oscillation model

On the left-hand side of Eq. (1), the first term means the inertia term, the second term corresponds to the damping force moment, and the third term denotes the restoring force moment. The fourth term represents the parametric resonance term which represents the effect of the gravity due to the mass of the blade. The term Ωt means azimuth angle ψ, and it is taken zero for the observed blade at the top of the rotor. The fifth term represents the flapwise moment due to centrifugal force. When the fourth and the fifth terms are transposed to the right-hand side, the right-hand side involves all moments due to the external forces.

The flapwise oscillation of the blade might bring about the influences on the flow field and the blade load through the two processes, namely, the coordinate change of the collocation points (the positions of blade panels) and the change of relative velocity to the blade section. The change in the relative velocity is represented by the oscillation velocity of the blade as,

$$y_b\dot{\boldsymbol{\beta}}_f = \left(0, \quad -y_b\dot{\beta}_f \sin\beta_f, \quad y_b\dot{\beta}_f \cos\beta_f\right) \qquad (2)$$

where y_b is the blade coordinate shown in Fig. 1. The boundary condition for flow analysis, which involves the coordinate change of collocation point due to the oscillation, can be written as follows,

$$\begin{aligned} &\left(\boldsymbol{W}'_{b,0} - \boldsymbol{\Omega}\times\mathbf{r}_b\cos\beta_f + \nabla\Phi - y_b\dot{\boldsymbol{\beta}}_f\right)\cdot\boldsymbol{n} = 0 \\ &\boldsymbol{W}'_{b,0} = \left(u_{b,0} \quad v_{b,0}\cos\beta_f + w_{b,0}\sin\beta_f \quad -v_{b,0}\sin\beta_f + w_{b,0}\cos\beta_f\right) \end{aligned} \qquad (3)$$

where $\boldsymbol{W}'_{b,0}$ is the uniform inflow velocity seen in the coordinate fixed to the oscillating blade, and u_b, v_b, and w_b represent relative velocity components to the blade. $\mathbf{r}_b$ and $\boldsymbol{\Omega}$ denote the position vector of the collocation point and the angular velocity vector of the rotor rotation, respectively. The vector $\boldsymbol{n}$ is the unit normal to the blade surface and Φ is the velocity potential. The subscript '0' corresponds to the values for the uniform inflow (see Figs. 1 and 2).

In order to solve Eq. (1) numerically, the Runge-Kutta method is adopted along with the initial condition that the flapping angle at time t=0 is β_f=β_{f0}=0[deg]. The flapwise fluid moment M_f =M_{f0} at t=0 is calculated by the aerodynamic load calculation without the blade oscillation. At the next time step t=t_1, the moment M_f=M_{f1} is calculated with the consideration of the blade oscillation by using Eq. (2). The flapping angle at t=t_1 is, then, calculated by Eq. (1) using M_{f0}, M_{f1}, and β_{f0}. By repeating this process, the instantaneous flapwise fluid moment M_f and the flapping angle β_f at each time step are calculated.

The preceding description shows that the flow field around the blade and the blade oscillation model are governed by the separate equations, and mutual interactions are taken into account, namely, the calculation systems for fluid and oscillation are coupled weakly in the present analysis.

2.4 Model Wind Turbine and Calculation Conditions

The configuration of the two-bladed model wind turbine used by NREL[13] is adopted for the calculation of the coupled analysis. With this turbine, NREL has performed a series of experiments in the large wind tunnel in NASA. The specification of the rotor blade is listed in Table 1 and its overview is shown in Fig. 3. More details such as the distributions of the chord length and twist angle of the blade are described in NREL's report[14]. The airfoil section of the blade is represented by NREL S809[14] for the whole span from the blade tip to the root. For the viscous correction, two dimensional airfoil characteristics[14] of NREL S809 is used, which was obtained by Ohio State University under the condition of Re=1.0×10^6.

The suction and pressure surfaces of the rotor blade are discretized in chordwise direction using the cosine spacing method so that the panels are dense near the leading edge of the blade. The spanwise panels are discretized similarly by the full-cosine spacing method. The number of panels and the azimuth step size are determined by regarding the analysis accuracy and the calculation time. In terms of the panel numbers, each blade is discretized into 8 panels in the chordwise direction and 10 panels in the spanwise direction, resulting in 160 panels for each blade, although no panel is allocated on the outer tip surface of the blade or the inner part of the blade root.

In order to examine the effect of the azimuth step size $\Delta\psi$, the aerodynamic load calculations have been conducted with three conditions of $\Delta\psi$=3.0, 5.0, 10.0[deg]. Each numerical calculation has been performed for the period of 20 revolutions of the rotor, so that the obtained calculation results corresponding to the final revolution posses sufficiently periodic nature. After 20 revolutions of the rotor, the wake panels shed from the blade at the initial stage of the calculation have flown downstream sufficiently far distant from the rotor plane.

The rotational speed of the rotor is kept 72 [rpm], which corresponds to the rotor angular speed of Ω=7.54 [rad/s], and the rotation frequency of f_R=1.2 [Hz]. The present calculation doesn't involve the pitch control of the blade.

Figure 4 shows an example of the calculated results for the structure of wake vortices released from a rotor blade under the yawed inflow condition. This is the result after the period of 15 rotor revolutions and doesn't include the wake vortex panels released at the initial stage. Due to the yawed inflow, the wake vortex structure is inclined to positive x direction, and in terms of induced velocity, the effect of the wake vortex on the rotor varies with the azimuth blade position. The wake vortex sheet is seen to roll up at the outer and the inner edges, since the wake vortices released from the spanwise positions near the root and tip have stronger circulation than those from the inboard sections of the blade. As the time goes by, the wake vortices experience a large deformation in their shape and show complex configuration.

In this study, the continuous deflection of the rotor blade is represented by a flapping angle of the hinge with one degree of freedom. In the oscillation calculation, the inertia moment in Eq. (1) is determined by referring the structural and mass data of the NREL model rotor, as $I=1.0\times10^3$[kgm^2]. Based on the assumption that the structural damping effect is much smaller than the aerodynamic damping effect for first mode oscillation[15], the structural damping coefficient is neglected (c_{ab}=0[N·m·s/rad]) in this study. The spring constant of the hinge, k, is set as eleven kinds of values as listed in Table 2, resulting in the variation of flapwise eigen frequency of rotor blade $f_b(=(1/2\pi)\sqrt{k/I}\,)$[Hz]. Actual NREL model rotor blade corresponds to the stiffest hinge spring condition of $k=211.0\times10^4$ [N·m/rad]. The ratio of the blade flapwise eigen frequency to the rotation frequency, f_b/f_R, represents the nature of the blade oscillation, and f_b/f_R=1, f_b/f_R<1 and f_b/f_R>1 correspond to the cases of resonant, soft blade, and stiff blade, respectively.

Table 1 Specifications of rotor blade[13]

Number of blade N_B	2
Radius R	5.029 [m]
Root cut off radius	0.250R
Blade length b	3.772 [m]
Preset angle θ_{tip}	3.0 [deg]
Tilt angle	0 [deg]
Coning angle	0 [deg]
Blade profile	NREL S809

Fig. 3 NREL wind turbine model[13]

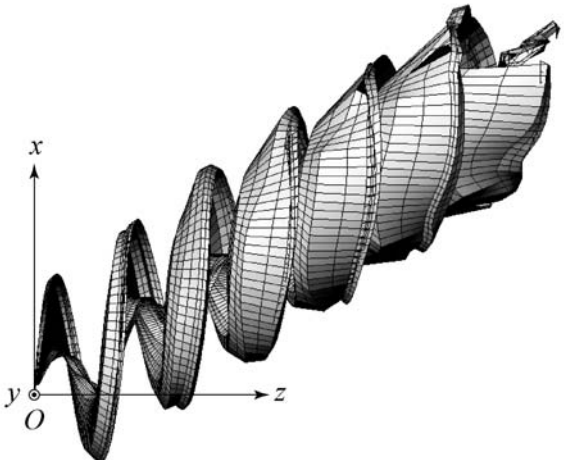

Fig. 4 Structure of vortex wake panels in a yawed inflow condition

Table 2 Oscillation ratio for various spring rate

Soft	$k^*\times10^4$	1.0	2.0	3.0	4.0	5.0	
	f_b/f_R	0.42	0.59	0.73	0.84	0.94	
Stiff	$k^*\times10^4$	8.0	13.0	23.0	43.0	80.0	211.0
	f_b/f_R	1.19	1.51	2.01	2.75	3.751	6.09

* unit: N·m/rad

3. Calculation Results and Discussions

3.1 Power Coefficient and Axial Drag Coefficient

In order to verify the validity of the aerodynamic load calculation model, the calculated results under no oscillation condition are compared with the experimental results[13] conducted by NREL. Figure 5 compares the calculated results (denoted as 'FWM' in Fig. 5) with the experimental results (as 'Exp.') for (a) power coefficient C_p ($=T\Omega/0.5\rho W_0^3\pi R^2$, T: rotor torque, ρ: density, Ω: rotor angular speed) and (b) axial drag coefficient C_{Dax} ($=D_{ax}/0.5\rho W_0^2\pi R^2$, D_{ax}: axial drag). They are plotted against the tip speed ratio λ ($=R\Omega/W_0$) for various yaw misalignment angle ϕ_y. In the definition of C_p and C_{Dax}, the swept area of rotor πR^2 was used. From Fig. 5 it can be said that the calculated C_p and C_{Dax} agree comparatively well with the experimental results, which confirms the validity of the aerodynamic load analysis model.

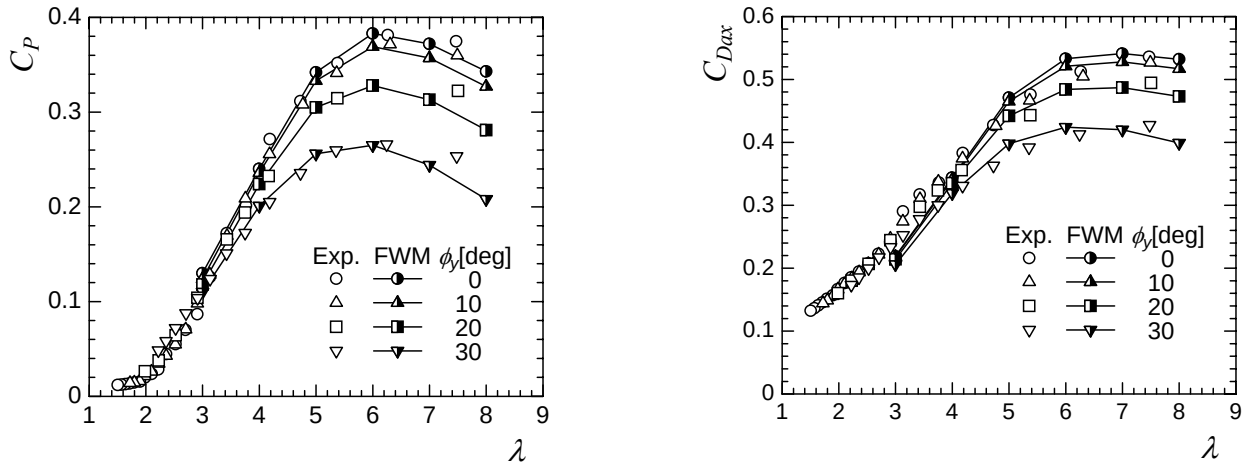

(a) Power coefficient (b) Axial force coefficient

Fig. 5 Comparison of power coefficient and axial force coefficient

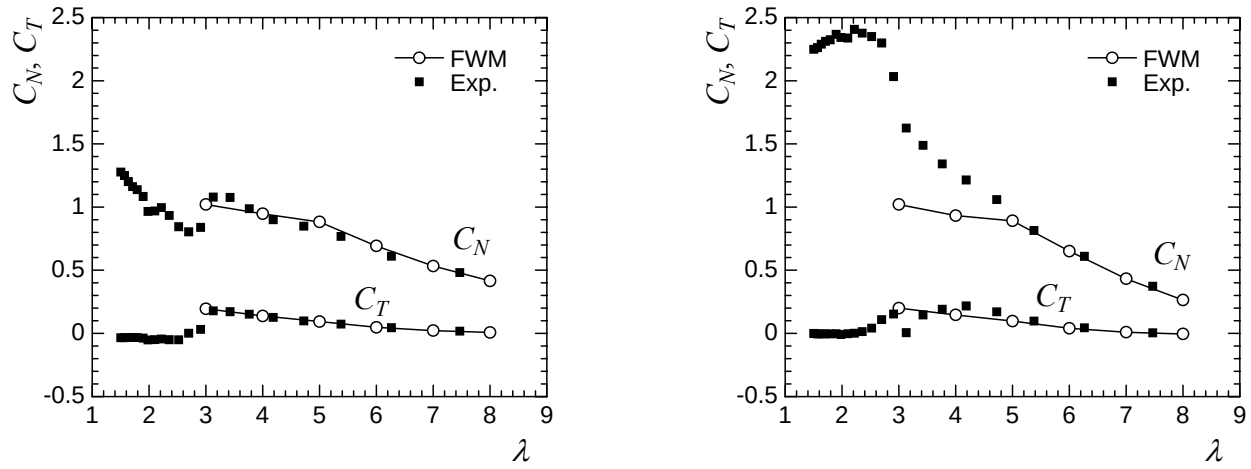

(a) At span position y_b/R=0.8 (b) At span position y_b/R =0.3

Fig. 6 Comparison of normal and tangential force coefficient in the case of ϕ_y=0deg

3.2 Normal Force Coefficient and Tangential Force Coefficient

Figure 6 shows the normal force coefficient C_N and the tangential force coefficient C_T exerted on the blade sections at the spanwise positions of y_b/R=0.8 and 0.3, for various tip speed ratio with the yaw misalignment of ϕ_y=0[deg] under no oscillation conditions. The coefficients C_N and C_T are defined and deduced in the following procedure. First, decompose the resultant force of lift and drag forces on the blade elements into the components normal and tangential against the chord line. Normalizing them by the dynamic pressure of the relative flow into the blade element, then we obtain C_N and C_T as shown in Fig.7. Although the lift and drag coefficients are usually used as the representative aerofoil characteristics, they are not appropriate for the wind turbine rotor blade because of the difficulty in the definition or measurement of the angle of attack to the rotating blade. Therefore it is better to discuss the aerodynamic characteristics of the blade section by using C_N and C_T, which can be defined straightly from the blade geometry[16].

At the spanwise position of y_b/R=0.8 (see Fig. 6(a)), where the flow around the blade seems to be nearly two dimensional, the calculated C_N and C_T agree well with the measurement results. At y_b/R=0.3, on the other hand, there exist recognizable differences between the calculated and experimental results for C_N at the tip speed ratio lower than 5, where the angle of attack is relatively large. This is mainly due to the fact that the present models for the viscous correction and the dynamic stall don't involve 3D boundary layer effects on the lift force enhancement near the blade root. The aerodynamic load near the spanwise position of y_b/R=0.8 is dominant in terms of torque and axial drag coefficient of the rotor, so that the power coefficient and axial drag coefficient shown in Fig. 5 comparatively agree with the measurement results even at low tip speed ratio. For other yaw misalignment angles, obtained distributions of C_N and C_T show similar tendency to those for ϕ_y=0[deg].

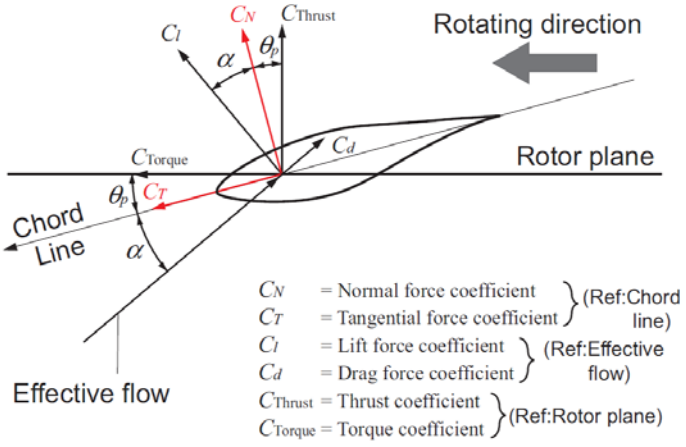

Fig. 7 Definitions of normal and tangential force coefficient

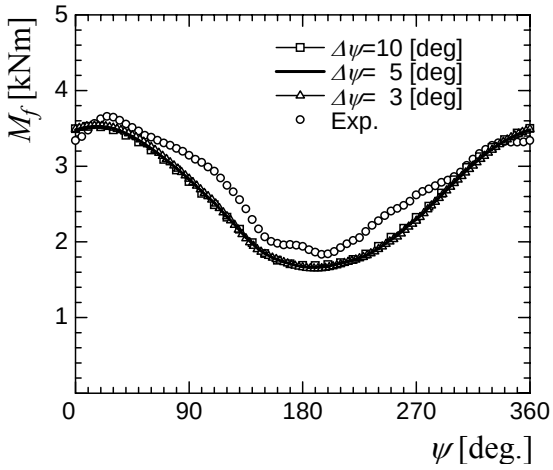

(a) W_0=13.0 m/s (λ=2.9)

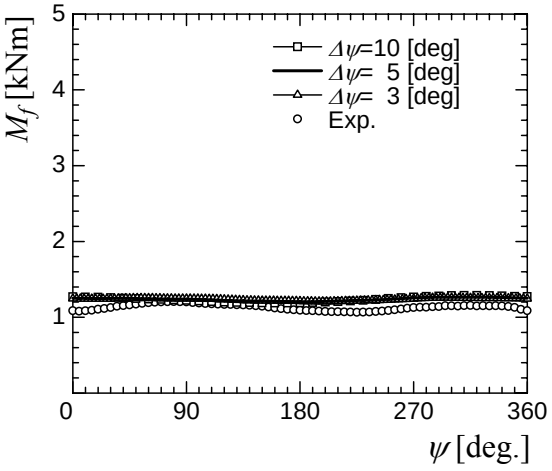

(b) W_0=6.1 m/s (λ=6.2)

Fig. 8 Comparison of flapwise fluid moment M_f in the case of ϕ_y=30deg

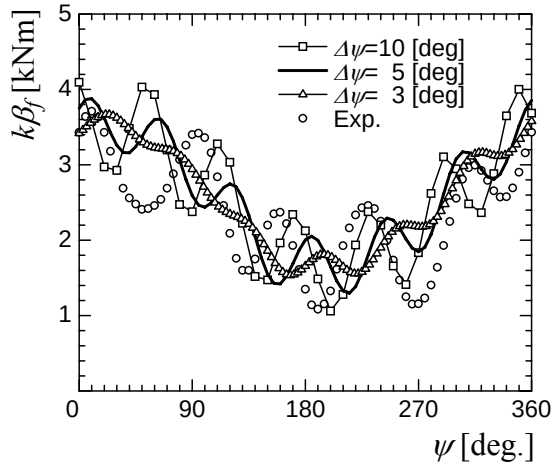

(a) W_0=13.0 m/s (λ=2.9)

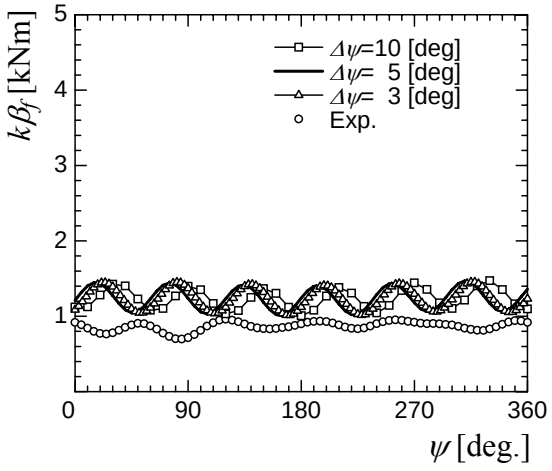

(b) W_0=6.1 m/s (λ=6.2)

Fig. 9 Comparison of flapwise bending moment $k\beta_f$ in the case of ϕ_y=30deg

3.3 Flapwise Moment

Before predicting the aerodynamic load on the blade rotor with soft structure, we have verified the validity of analysis model including oscillation model by comparing the calculated results with the measurement for the model turbine, which has comparatively stiff structure. Here, the results obtained at λ=2.9 (W_0=13.0[m/s]), which is stall region and at λ=6.2 (W_0=6.1[m/s]), which is maximum efficiency point, are shown about the flapwise oscillation occurring under the condition that yaw misalignment angle ϕ_y=30[deg].

Figures 8 and 9 show the calculated results of flapwise fluid moment M_f and the flapwise bending moment exerted on the structural system $k\beta_f$ plotted against the azimuth position of the blade ψ, in comparison with the measurement results[13]. The inflow wind speed W_0 for the calculation was settled at the same values as those for the experiment and the corresponding tip speed ratios λ were also inscribed. In order to examine the effect of azimuth step size $\Delta\psi$ on the calculation, the calculated results for $\Delta\psi$ = 3, 5, 10[deg] were shown in Figs. 8 and 9. The blade structure for the NREL model wind turbine rotor has the first flapwise eigen frequency of f_b=7.25[Hz] and the calculation has been done with the numerical structural model with the same flapwise eigen frequency. There are two kinds of experimental results for the flapwise moment served by the NREL's measurement. The one was the flapwise moment obtained by integrating the static pressure distributions measured over the blade surface. The other flapwise moment was directly measured by strain gages installed near the blade root. These flapwise moments correspond to the calculated flapwise fluid moment M_f and flapwise bending moment $k\beta_f$, respectively. The calculated results shown in Figs. 8 and 9 are the ensemble averages of the flapwise moments at azimuth angle of the blade, ψ. They have been averaged over the collection of the calculation results obtained from 15th to 20th revolutions, where the blade oscillation gets settled at quasi-periodic state. The measurement results are also averaged for the locked-phase of the blade azimuth with the increment of $\Delta\psi$=5[deg].

The effect of azimuth step $\Delta\psi$ on the calculated flapwise fluid moment M_f is hardly seen from Fig. 8, and the calculated M_f agrees well with the measurement, which shows the validity of the estimated unsteady aerodynamic load by present calculation method.

The flapwise bending moment on the structural system $k\beta_f$, in contrast, shows recognizable differences between the calculation

and the measurement both in the average value and frequency characteristics as shown in Fig. 9. In particular at λ=2.9, the difference of azimuth step $\Delta\psi$ significantly affects the calculation results. When $\Delta\psi$ is as large as 10[deg], the amplitude of the calculated flapwise bending moment change gets close to the measurement results although its frequency characteristic is different from the measurement. When $\Delta\psi$ is taken as small as 3[deg], the calculated results shows similar frequency characteristic to the measurement results although its amplitude becomes smaller than the measurement. The reasons for these results are thought that a simple model with one degree of freedom was adopted for the blade structure and its damping coefficient, c_{ab}, was assumed to be zero for the present calculation.

Hereafter, the calculation results with $\Delta\psi$=5[deg] will be used for further discussion, since the azimuth step gives relatively little effect, especially for the condition of large tip speed ratio.

3.4 Effects of Blade Stiffness

In order to examine the effects of the blade stiffness, namely, the eigen frequency of the rotor blade, f_b, on the flapwise moment, the calculated flapwise fluid moment M_f and the flapwise bending moment on the structural system $k\beta_f$ are plotted against f_b, in Figs. 10 and 11, when soft structural design is adopted to the rotor blade. Figure 10 shows the changes of average and standard deviation of the flapwise fluid moment M_f against frequency ratio f_b/f_R, where f_R is the rotation frequency of the rotor, obtained for the operating conditions of (a) λ=3 and (b) λ=6, with the yaw misalignment angle of ϕ_y=30[deg]. The flapwise bending moment $k\beta_f$ is shown in Figs. 11(a) and (b) in the same way as Figs. 10(a) and (b). The arrows in the figures indicate vertical axes of reference for respective plotted lines. The ordinates are normalized by the averaged value of the flapwise fluid moment $\overline{M}_{f\infty}$, which has been calculated for the rotor blade with infinite stiffness.

It can be found from Figs. 10 and 11 that the averages of M_f and $k\beta_f$ slightly decrease for the soft blade of f_b/f_R<1 as much as 5~7%, compared with the fully stiff blade, while they are almost unchanged for the blade of f_b/f_R>1.

As seen from the standard deviations of the moment fluctuations, the amplitude of the flapwise bending moment is larger than that of the flapwise fluid moment for the blade of f_b/f_R>1. The resonant blade (f_b/f_R=1) at the low tip speed ratio λ=3, in particular, shows extremely large amplitude. The soft blade of f_b/f_R<1, in contrast, shows fairly decreased fluctuation of the flapwise load, which is more noticeable at tip speed ratio lower than the optimum operating condition. The soft structure can, however, reap the benefit of the load reduction only at the operating condition of the rated rotor speed. Since the variable speed rotor and the

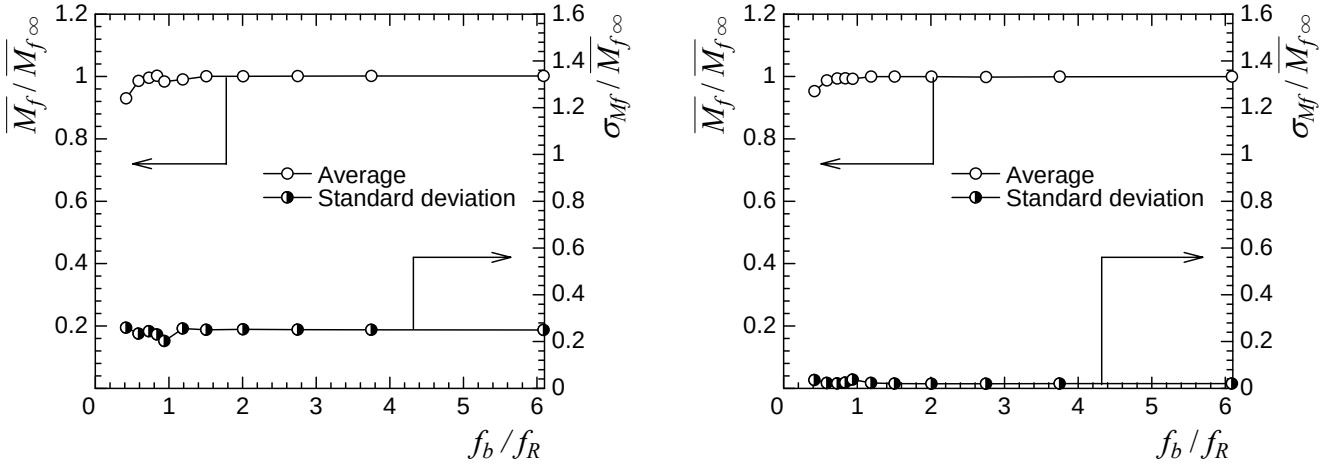

(a) λ=3 (b) λ=6

Fig. 10 Comparison of flapwise fluid moment M_f for non-dimensional frequency f_b/f_R in the case of ϕ_y=30deg

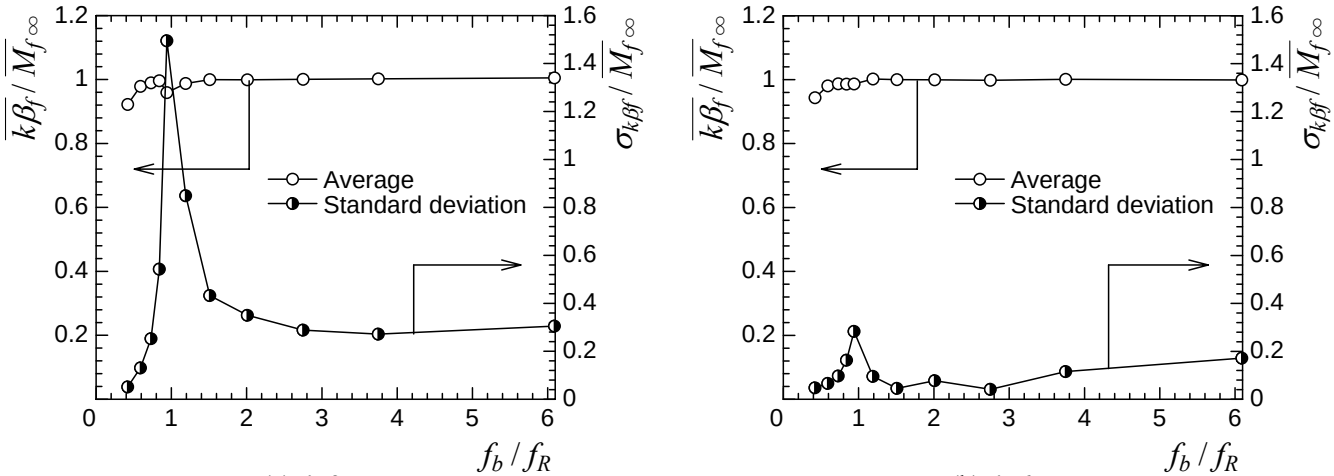

(a) λ=3 (b) λ=6

Fig. 11 Comparison of flapwise bending moment $k\beta_f$ for non-dimensional frequency f_b/f_R in the case of ϕ_y=30deg

constant speed rotor at starting and/or stopping stage might experience the resonance points of the soft structure, the operational scheme for those rotors has to be designed carefully.

The effect of adapting soft structure for the blades on the power output from the rotor is examined at the end of the section. The change of power coefficient, C_p, is plotted against the frequency ratio of the blade, f_b/f_R, in Fig. 12, at the yawed operation with ϕ_y=30[deg], for the tip speed ratios of λ=3 and 6. It can be found from the figure that C_p decreases slightly for the soft structure rotor of f_b/f_R<1. This can be attributed to the decreased swept area of the rotor due to the flapwise inclination of the soft blade to the downstream in average. Therefore, careful attention has to be paid for choosing the appropriate eigen frequency of the rotor blade from the viewpoints of the fluid and structural systems, when the soft structural design is to be adopted for the wind turbine rotor.

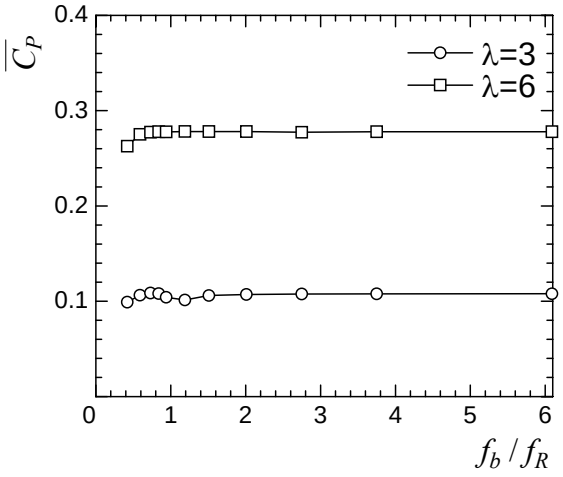

Fig. 12 Comparison of averaged power coefficient C_P for non-dimensional frequency f_b/f_R in the case of ϕ_y=30deg

4. Conclusions

Fluid-structure weak coupled analysis has been performed for NREL model wind turbine in yawed inflow conditions, using free wake panel method and an oscillation blade model with one degree of freedom. Along with validity evaluation of the present calculation model, the effect of soft structural design of the blade on the dynamic characteristic of the wind turbine rotor has been examined in this paper. The obtained major results are listed below.

(1) The present simple model based on hinge-spring for the flapwise oscillation of the rotor blade is proved to possess certain level of validity, for the fluid-oscillation coupled analysis, since the results of numerical analysis agree well with the measurement results.
(2) The flapwise fluid moment and flapwise bending moment on the rotor blade were analyzed numerically by adopting the flapwise eigen frequency (elastic coefficient) of the blade as a parameter, and the effect of soft blade was found on the decrease of the flapwise bending moment.
(3) In order to prevent the resonant oscillation of the blade and the decrease in the turbine power due to excessive softness of the blade, appropriate eigen frequency of rotor blade has to be chosen, from the viewpoints of the fluid and structural systems, when the soft structural design is to be adopted for the wind turbine rotor.

While the present calculation model adopts a simple oscillation model for the blade with one degree of freedom, the actual elastic blades show oscillatory deflection continuously distributed in the spanwise direction. Thus, more sophisticated modeling is inevitable for the blade structure, in order to predict the fluid coupled oscillation more precisely.

Acknowledgments

The authors wish to thank NREL, especially Dr. Schreck, for providing us their valuable experimental data.

Nomenclature

c	Local chord length [m]	$\boldsymbol{r}_b$	Position vector of the collocation point [m]
c_{ab}	Structural damping coefficient [N·m·s/rad]	Re	Reynolds number [-]
C_{dax}	Axial drag [N]	t	time [s]
c_{dvis}	Drag coefficient involving the viscous effects [-]	T	Rotor torque [N·m]
c_{linv}	Local lift coefficient deduced by Kutta-Joukowski theorem [-]	u_b, v_b, w_b	Relative velocity components to the blade [m/s]
		U_R	Relative wind speed to the blade section [m/s]
c_{lvis}	Lift coefficient involving the viscous effects [-]	$\boldsymbol{W}'_{b,0}$	Uniform inflow velocity [m/s]
C_N	Normal force coefficient [-]	β_f	Instantaneous flapping angle [rad]
C_p	Power coefficient [-]	γ, Γ	Circulation [m^2/s]
C_T	Tangential force coefficient [-]	$\Delta\psi$	Azimuth step size [rad]
D_{ax}	Axial drag coefficient [-]	λ	Tip speed ratio [-]
f_b	Flapwise eigen frequency of rotor blade [Hz]	ρ	Fluid density [kg/m^3]
f_R	Rotation frequency [Hz]	Φ	Velocity potential [m^2/s]
g	Acceleration of gravity [m/s^2]	ϕ_y	Yaw misalignment angle [rad]
I	Moment of inertia of the blade [kg·m^2]	ψ	Azimuth angle of the blade [rad]
k	Spring constant of the hinge spring [N·m/rad]	Ω	Rotor speed [rad/s]
M_f	Flapwise fluid moment due to the aerodynamic load [N·m]	$_0$	Subscript corresponding to the values for the uniform inflow
$\boldsymbol{n}$	Unit vector normal to the blade surface [m]		
R	Rotor radius [m]		

References

[1] IEA, *IEA Wind Annual Report 2005*, 2006.

[2] Jonkman, J.M. and Buhl Jr., M.L., *FAST User's Guide*, National Renewable Energy Laboratory, NREL/EL-500-38230, 2005, p. 125.

[3] Guinta, A. A., 1997, "Aircraft Multidisciplinary Design Optimization Using Design of Experimental Theory and Response Surface Modeling Methods," Ph. D. Thesis, Department of Aerospace Engineering, Virginia Polytechnic Institute and State University, Blacksburg, VA.

[4] Bossanyi, E.A., *Bladed for Windows – Theory Manual*, Garrad Hassan & Patners Limited, Bristol, England, Document No. 282/BR/009. Issue No. 3, 1997, p. 54.

[5] de Vries, O., Comment on the Y*aw Stability of a Horizontal-Axis Wind Turbine at Small Angles of Yaw*, Wind Engineering, Vol. 9, No. 1, 1985, pp. 42-49.

[6] Duque, E. P. N., van Dam, C. P., *et al*., *Navier-Stokes Analysis of Time-Dependent Flows about Wind Turbines*, Proc. 3rd ASME/JSME Joint Fluids Engineering Conference, San Francisco, FEDSM99-7814, 1999.

[7] Huyer, S. A., Simms, D, and Robinson M. C., *Unsteady Aerodynamics Associated with a Horizontal-Axis Wind Turbine*, AIAA Jouranl, Vol. 34, No. 7, 1996, pp. 1410-1419.

[8] Bierbooms, W. A. A.M., *A Comparison between Unsteady Aerodynamic Model*, Proc. European Wind Energy Conference, Amsterdam, 1991, pp. 13-17.

[9] Imamura, H., Takezaki, D., Hasegawa, Y., et al, Study on Unsteady Flow around a HAWT Rotor by Panel Method (Calculation of Yawed Inflow Effects and Evaluation of Angle of Attack in the Three-Dimensional Flow Field), JSME, 71-701(B), 2005, pp. 154-161.

[10] Leishman, J.G., *Challenge in Modeling the Unsteady Aerodynamics of Wind Turbines*, AIAA2002-0037, 2002.

[11] Matsumiya, H., Kawamura, S. and Tanaka, H., *Design and Behaviour Analysis of a Mechanical Governor for a Variable-Speed Wind Turbine Generator*, JSME, 56-529(C), 1990, pp. 2373-2377.

[12] Shimizu, Y., Kamada, Y. and Tobinaga, I., *Studies on Horizontal Axis Wind Turbine with Passive Teetered Brake and Damper Mechanism : (Relationship between Braking Effect of Rotor Blade and Flow Patterns around Rotor)*, JSME, 65-633(B), 1999, pp. 1696-1702.

[13] Hand, M.M., Simms, D.A., *et al*., *Unsteady Aerodynamics Experiment Phase VI: Wind Tunnel Test Configurations and Available Data Campaigns*, NREL/TP-500-29955, 2001.

[14] Simms, D.A., Hand, M.M., Fingersh, L.J. and Jager, D.W., *Unsteady Aerodynamics Experiment Phases II-IV. Test. Configurations. and Available Data. Campaigns*, NREL/TP-500-25950, 1999.

[15] Burton, T., Sharpe, D., *et al*., *Wind Energy Handbook*, John Wiley & Sons Ltd., 2001, pp. 262-264

[16] G.A.M. van Kuik, R.P.J.O.M van Rooij and Hiroshi Imamura, *Analysis of the UAE Phase VI Wind Tunnel Results in the Non-Yawed Flow*, 2004 European Wind Energy Conference and Exhibition, Nov. 22-26, 2004, London, pp. 1-11.